Polarization dynamics of femtosecond pulses propagating in air

M. Kolesik
Arizona Center for Mathematical Sciences, Department of Mathematics, University of Arizona, Tucson, AZ 85721.
and
Institute of Physics, Slovak Academy of Sciences, Bratislava, Slovakia

J.V. Moloney and E.M. Wright
Arizona Center for Mathematical Sciences, Department of Mathematics, University of Arizona, Tucson, AZ 85721.
and
Optical Sciences Center, University of Arizona, Tucson, AZ 85721.
(February 2, 2008)

arXiv:physics/0101073v1 [physics.optics] 17 Jan 2001

Polarization dynamics of femtosecond light pulses propagating in air is studied by computer simulation. A rich variety of dynamics is found that depends on the initial polarization state and power of the pulse. Effects of polarization on the plasma and supercontinuum generation are also discussed.

I. INTRODUCTION

There has been a great interest in long distance femtosecond pulse propagation in air in recent years motivated in part by potential applications in remote sensing and laser-induced lightning. The first experimental observations [1,2] of highly localized, high-intensity filaments propagating over distances that exceed their corresponding Rayleigh lengths by orders of magnitude motivated the efforts to understand the phenomenon [3–8]. Due to the violent formation process, and the extreme time and spatial scales of the filaments, the computer simulations and analytic approaches turned out to be vital tools to grasp the underlying physics [9–16]. Several models have been proposed. The first explanation suggested a stationary waveguide formed by competing effects of nonlinear self-focusing and linear defocusing by underdense plasma generated in the most intense part of the pulse [1]. An alternative model employed a notion of the "moving focus" to explain how the geometrical focus of a beam is transformed into a long filament [3]. More recently, a dynamic spatial replenishment model emerged from numerical investigation by Mlejnek et al. [9,10]. The essential feature of the femtosecond propagation of infrared (IR) pulses is its dynamics that makes it possible that the localized filaments propagate over long distances and do not suffer significant energy loses. The basic mechanism involves a dynamic balance between the nonlinear self-focusing and defocusing by free electrons generated via multi-photon absorption by the high-intensity filaments. When the self-focusing leading edge of the pulse starts to generate plasma, it thus creates a defocusing "lens" for the trailing portion of the pulse. This has two effects; First, it limits the losses due to absorption in the plasma and, second, it prevents the major portion of the pulse from experiencing self-focusing collapse. After the plasma generating leading portion of the pulse exhausts its energy, the strength of the defocusing lens decreases, and the self-focusing starts over again, this time in the "next temporal slice" of the pulse. The whole process can repeat several times, depending on the total energy of the pulse. The qualitative features of the dynamical spatial replenishment remain valid also in transversely wide pulses, that break-up into multiple filaments [12].

Up to the present, most of the work on the experimental side and all numerical studies have been concerned with the case of linearly polarized input pulses. Recently, Petit et al. [17] studied the effects of the polarization on the propagation of femtosecond IR pulses. They have measured luminescence from the plasma generated in the filaments to show that the polarization of the pulse plays an important role in the plasma generation. Due to the highly dynamic nature of the filament formation and propagation, it is natural to expect a rich polarization dynamics in femtosecond pulses. In this initial study, we restrict ourselves to femtosecond pulses with modest peak powers that retain their initial radial transverse symmetry and are just sufficient to produce several refocusing events within a single pulse. The initial polarization of the pulse is varied and the polarization state is recorded along the propagation path. Our results indicate a tight correlation between the evolution of the pulse waveform along the propagation distance and certain global polarization parameters. Thus, the measurements of the polarization state could provide yet another tool to extract information on dynamics of pulses as well as an opportunity to correlate experiment and theory.

The remainder of the paper is organized as follows. Our basic model is described in Sec. II, and details of our simulated experiment are given in Sec. III. Plasma production, polarization dynamics, and the associated supercontinuum generation are then discussed in Secs. IV-VI. Finally, our summary and conclusions are given in Sec. VII.

II. MODEL EQUATIONS

Since the typical transverse dimension of the self-focusing collapsing filaments are a few tens to hundred microns in the IR wavelength region, it is a good approximation to consider the optical field as transverse. We describe the complex optical amplitude in terms of two circularly polarized components, $\mathcal{E}^{\pm}$. The choice of the circularly polarized basis is motivated by the fact that in this basis the nonlinear birefringence is "diagonal" and preserves the power in each component, which in turn makes its implementation easier. Our model is a straightforward extension of the scalar version we used in our previous studies [9,12]. It takes into account the effects of diffraction, normal group velocity dispersion (GVD), multi-photon ionization (MPI) and avalanche plasma generation, defocusing of light by the generated free electrons, and instantaneous and delayed cubic nonlinearity:

$$\begin{aligned}\frac{\partial \mathcal{E}^{\pm}}{\partial z} &= \frac{i}{2k}\nabla_{\perp}^2\mathcal{E}^{\pm} - \frac{ik''}{2}\frac{\partial^2\mathcal{E}^{\pm}}{\partial t^2} \\ &-\frac{\sigma}{2}(1+i\omega\tau)\rho\mathcal{E}^{\pm} - \frac{\beta^{(K)}}{2}|\mathcal{E}|^{2K-2}\mathcal{E}^{\pm} \\ &+i\frac{2\omega}{3c}(1-f)n_2(|\mathcal{E}^{\pm}|^2+2|\mathcal{E}^{\mp}|^2)\mathcal{E}^{\pm} \\ +i\frac{2\omega}{3c}fn_2&\left[\int_{-\infty}^{\infty}dt'R(t-t')(|\mathcal{E}(t')^{\pm}|^2+2|\mathcal{E}(t')^{\mp}|^2)\right]\mathcal{E}^{\pm} \quad .\end{aligned} \tag{1}$$

Here ω is the optical frequency, $|\mathcal{E}|^2 = |\mathcal{E}^+|^2 + |\mathcal{E}^-|^2$ the combined intensity of the two circularly polarized components, $k = \omega/c$, $k'' = \partial^2 k/\partial\omega^2$, ρ is the electron density, σ is the cross-section for inverse bremsstrahlung, τ is the electron collision time, $\beta^{(K)}$ is the K-photon absorption coefficient, and the nonlinear change in refractive-index for a linearly polarized continuous wave (cw) field is $n_2|\mathcal{E}|^2$. The corresponding critical power for self-focusing collapse for linearly polarized fields is $P_{cr} = \lambda_0^2/2\pi n_2$, or P_{cr} =1.7 GW for our parameters. In contrast, the critical power for self-focusing for circularly polarized fields $P_{cr}^{\pm} = 1.5P_{cr}$ is 1.5 times that for linearly polarized fields [18]. The normalized response function (characterized by the resonance frequency Ω and the decay Γ)

$$R(t) = \theta(t)\,\Omega^2\,e^{-\Gamma t/2}\,\frac{\sin(\Lambda t)}{\Lambda}\,, \qquad \Lambda = \sqrt{\Omega^2 - \Gamma^2/4}\,, \tag{2}$$

accounts for delayed nonlinear effects, and f is the fraction of the cw nonlinear optical response which has its origin in the delayed component, and we denoted the Heaviside step function by $\theta(t)$. In the present model, we chose the relative weight of the "self" and "cross" non-linear birefringent terms the same as for the instantaneous Kerr effect and nonlinear Raman effect, namely, the cross effect has a weight twice that of the self effect as is appropriate for an isotropic medium [18].

The optical field amplitude equations are completed by a simple equation describing the evolution of the plasma density:

$$\frac{\partial\rho}{\partial t} = \frac{\sigma}{E_g}\rho|\mathcal{E}|^2 + \frac{\beta^{(K)}|\mathcal{E}|^{2K}}{K\hbar\omega} - a\rho^2\,, \tag{3}$$

where the first and second terms represent the avalanche and multi-photon effects, while the last one models the plasma recombination. Note, that at the time-scales relevant for the present study, the only practically important contribution comes from the the multi-photon term. For the pulse powers we use, it is sufficient to include oxygen alone as a source for MPI, since its corresponding multi-photon order is lower than that for nitrogen. We use the Keldysh theory formula to calculate the MPI rate [19].

Explanations of symbols that appear in our model equations are listed in Table 1 together with the values used in our simulation.

III. NUMERICAL SIMULATION

To study the role of the initial polarization state of the pulse on its subsequent propagation, we performed a series of simulations. In all runs, the initial pulse was chosen to be a Gaussian wave-packet (in time and space) characterized through its central wavelength λ = 775 nm, pulse waist w = 0.7 mm and temporal duration $\tau_{\rm FWHM}$ = 200 fs. We fixed the initial peak intensity as 1.0×10^{16} W m^{-2} which is a relatively modest value: for a linearly polarized input this corresponds to an input peak power of $P = 7.7$ GW$= 4.5P_{cr}$, whereas for a pure circular polarization $P = 7.7$ GW$= 3.0P_{cr}^{\pm}$. At these powers, there are typically two to three refocusing events in the pulse propagation, and the numerics can be reliably controlled. At higher powers under a perfect axial symmetry of the pulse, it may be necessary to extend the model beyond the nonlinear Schrödinger equation (NLSE), and to include correction terms that allow to handle pulses with a very broad spectrum. To check our numerical procedures and model implementation, we performed most of the runs in two or three different resolutions. The data we present were obtained with the time-domain resolution of 0.24 fs. This resolution is sufficient to capture spectra several hundredth of nanometers wide. We provide more details of our testing procedures concerning the spectral resolution and algorithm validity in Sec. VI devoted to supercontinuum generation.

Below, we present our results for a series of runs that differ in the initial polarization state of the pulse. We change the polarization from the linear, through elliptic to circular, to see how it affects the dynamics of the filaments. In previous work on nonlinear propagation in fibers, the Stokes parameter formalism has been employed to classify the polarization dynamics for plane wave fields [20]. Here we employ space and time averaged Stokes parameters (s_0, s_1, s_2, s_3) as a description of the polarization dynamics of the propagating pulses. In particular, our Stokes parameters are calculated numerically according to the prescription

$$
\begin{aligned}
s_0 &= (\mathcal{F}_{\pi/2} + \mathcal{F}_0) \\
s_1 &= (\mathcal{F}_{\pi/4} - \mathcal{F}_{-\pi/4})/s_0 \\
s_2 &= (\mathcal{F}_{\pi/2} - \mathcal{F}_0)/s_0 \\
s_3 &= (\mathcal{F}_{\mathrm{CR}} - \mathcal{F}_{\mathrm{CL}})/s_0
\end{aligned} \tag{4}
$$

where $\mathcal{F}_\beta$ is the total energy detected after passing the pulse through a polarizer of state β

$$
\mathcal{F}_\beta = 2\pi \int_{-\infty}^{+\infty} \int_0^R |\mathcal{E}_\beta|^2(r,t) r dr dt \tag{5}
$$

with $\mathcal{E}_\beta$ the field resolved along the polarizer direction, and R the radius of a detection aperture chosen to select the the most intense region of the pulse around the filament. For a linear polarizer β is the angle of the polarizer, whereas for a circular polarizer $\beta = CR, CL$ corresponding to right and left circular polarization settings. Here we chose $R = 0.1$ mm, and perform the measurement of the Stokes parameters "in the near field". We note that s_0 is the total energy of the pulse detected over the aperture, and the remaining Stokes parameters are calculated as differences between the detected energy with different polarizer settings normalized to the total energy. Thus our prescription has a direct experimental interpretation and should therefore be of utility. The above prescription for determining the Stokes parameters also reduces to the usual definitions in the limit of long pulses of broad transverse extent.

In the numerical simulations to be presented we fix the initial Stokes parameter s_2 equal to zero, and vary s_1 and s_3 between zero and one to vary the initial polarization from linear through elliptic to pure circular polarization. Besides the polarization state, we also recorded the data pertaining to the plasma generation inside the pulse, and generation of the supercontinuum light. We start our discussion with plasma generation.

IV. PLASMA PRODUCTION

As the femtosecond pulse undergoes multiple self-focusings, the amount of plasma generated by its high-intensity portions reflects the spatio-temporal shape of the pulse. The total number of generated electrons as well as the maximal plasma densities exhibit peaks along the propagation distance. These peaks coincide with the locations of self-focusing collapses within the pulse, each peak being produced by a different temporal portion of the pulse. Figure 1 shows the plasma generation for three different initial polarizations of the pulse. The trend that one can see is quite in line with what is expected based on the functional form of the nonlinear birefringence. Namely, as we change the initial polarization from linear through elliptic to circular, the amount of the generated plasma decreases. Also, the onset of filament formation is delayed for the circularly polarized pulse because the critical power for self-focusing is higher for circularly polarized pulse as noted earlier. In other words, keeping the input peak power the same for different polarizations, we effectively decrease the self-focusing power of circularly polarized pulses. This is also the reason why the number of refocusing events can be higher in a close-to-linear or linear polarization than in a circularly polarized pulse. While the overall plasma production depends on the polarization state, the typical dimensions of the filaments are not very sensitive to it. That can be seen from the Figure 1 which shows the longitudinal extent of the plasma columns. The transverse dimensions of the plasma channels can be estimated from the ratio of the two curves shown in the figure as the square root of the ratio between the total number of electrons and the maximal plasma density. This characteristic dimension of the plasma channel is shown in Fig. 2 for three different polarizations. Though there are small variation between different initial polarizations, the thickness of the plasma channels is always roughly 60 microns in the most dense parts. The plasma channel generated by the circularly polarized pulse seems to be more "homogeneous", exhibiting less thickness variation along the propagation distance.

V. POLARIZATION DYNAMICS

While the dynamics of the plasma generation and its dependence on the polarization described in the previous Section is straightforwardly linked to the structure of the equations governing the optical field evolution, the polarization dynamics seems to be more difficult to interpret. Figures 3,4,5 show the Stokes parameters and the polarization degree as functions of the propagation distance for the three different initial polarizations we discussed in the previous Section. An interesting feature is the difference between the "stability" of initial linear and circular polarization. Figure 3 shows that a small perturbation to the linear polarization in the initial pulse leads to an increasing deviation of the polarization state from the initial one. In this sense, the linear polarization appears to be unstable, as the polarization measured after the filament formation can significantly differ from the initial one. Naturally, the rate of divergence for two close but not identical initial conditions decreases with the decreasing input power. On the other hand, in the case of almost circular polarization shown in Fig. 4, the pulse polarization state doesn't change that dramatically. Though there is a small decrease of the polarization degree, one can say that final polarization stays close to the initial one even after two refocusings of the pulse. Thus, the circular polarization seems to be more stable against small perturbations than the linear polarization. Figure 5 shows an interesting case of an initially elliptic polarization. Note that the Stokes parameter s_3, which measures the degree of circular polarization, only exhibits small variations, while the other two parameters decrease significantly after their initial increase in the first collapse.

That means that the light focused in the second collapse is predominantly circularly polarized. This observation is confirmed by examining the spatio-temporal polarization pattern within the pulse. This is an observation that may not be expected based on the previous results concerning cw self-focusing of polarized pulses [21,18]. Namely, in a situation close to a continuous wave regime, one can argue that the weaker circular component experiences a stronger focusing "lens" because of the factor two in the birefringence cross-term, and that eventually leads to equal intensities of both circular components and, therefore, linear polarization of the central filament. However, the important point here is that the femtosecond light filaments under consideration are extremely dynamic objects. The resulting polarization distributions strongly depend on the spatial and temporal location within the pulse, and any interpretation based on steady-state-like considerations becomes invalid. Namely, there is a delay between when the light encounters the focusing "lens" and when it actually reaches the focus. This delay interferes with the temporal profile of the pulse, which typically exhibits multiple peaks that may be just a few femtosecond long. As a consequence, the above simple argument is not sufficient to capture all essential features of the phenomenon. The tendency of the predominantly circular polarization of the most intense portion of a filament was also observed in our simulations that were not restricted to axial symmetry [22]. A wide beam with a random perturbation breaks up into multiple filaments that exhibit polarization properties similar to those we discuss here. However, one has to keep in mind, that in both cases, axisymmetric as well as fully spatially resolved, our simulation modeled pulses with relatively small energy fluence when compared to some current experiments. Therefore, it would be extremely interesting to see what happens to the polarization of the central filament in a pulse that has enough energy for many self-focusing events and also has the transverse profile clean enough to preserve its axial symmetry.

We conclude this Section with yet another presentation of the polarization dynamics data we have shown above. Namely, we want to show that the polarization changes closely reflect the self-focusing events within the pulse and, consequently, the locations where most of the plasma is generated. Figure 6 shows the root-mean-square rate of the change of the Stokes vector along the propagation distance

$$\frac{ds}{dz} = \sqrt{\left(\frac{ds_1}{dz}\right)^2 + \left(\frac{ds_2}{dz}\right)^2 + \left(\frac{ds_3}{dz}\right)^2} \qquad (6)$$

for the case of elliptic initial polarization of the pulse. The curve shown corresponds to the data depicted in Fig. 5 and in Fig. 1b). Note, that the maxima of the rate of the polarization change closely follow those in the plasma production curve. We thus see that the multiple self-focusing events in the single pulse leave their signature on the polarization. This could provide another way, besides the indirect plasma density observations [8,23–25], to visualize the dynamics of the spatial replenishment.

VI. SUPERCONTINUUM GENERATION

After contrasting the behavior of pulses polarized close to linear and circular from the points of view of plasma generation and of their polarization dynamics, we want to discuss the effects of polarization on the supercontinuum generation. However, before presenting our results, we feel a note concerning some technical questions is in order. The explosive spectral broadening in the supercontinuum generation in femtosecond pulses is a rather subtle phenomenon from the point of view of numerical simulation. Clearly, one needs a sufficient resolution in the time (spectral) domain to capture the broad spectrum, but the resolution may not be the only issue here. One has to check how broad is the spectral region within which the model and its numerical implementation describes the wave propagation correctly. It is expected, that at extreme powers, correction terms beyond the basic NLSE (see e.g. Ref. [26]) need to be included in the field equation. To ensure that we work in the regime where the correction terms may be neglected, and to assess the spectral band over which our numerics works well, we performed some comparative simulations. The choice of the reference frequency (wavelength) around which the NLSE is built is in principle arbitrary, though it is obviously most appropriate to choose it close to the central frequency of the modeled pulse. This means, that simulations that only differ in the choice of the reference frequency should give the same results. We have compared simulation with the reference frequency shift of 150 nanometers off the central wavelength of the pulse, and obtained a very close match of the spectra in the region from 500 to 1200 nm and over four decades in spectral intensity. Thus, in this interval we can trust the spectra extracted from our simulations. We would like to point out that this is in fact a rather strong test for the overall numerical implementation of the solver. But most important, the close agreement between the spectra shows that the correction terms beyond NLSE do not play an important role in our regime of modest input powers; This is because one can interpret them as corrections that partially restore the invariance of the original wave equation with respect to the choice of the (physically meaningless) reference frequency – that is exactly what our test shows is not needed for the conditions in our simulations.

Figure 7 shows comparison of the spectral broadening of two pulses that differ only in their initial polarization. The way we extracted the spectra from the pulse waveforms corresponds to measurement in a near field with the same aperture we used for polarization characterization. The figure shows spectra "measured" after the last self-focusing collapse, after which the pulse will eventu-

ally diffract and there will not be more supercontinuum generation. One can see that the pulse which was initially polarized close to linear exhibits a much stronger supercontinuum generation. However, note that we compare pulses with the same peak power, and what we see here is an effect similar to the plasma generation. Supercontinuum generation strongly depends on the available power and the natural measure of that power is in units of critical power for self-focusing. From that point of view the circularly polarized pulse is weaker and that is the main reason that it exhibits less spectral broadening. However, this situation represents a reasonable experimental setup in which only the polarization is changed.

To get a feeling regarding the role of the group velocity dispersion in the supercontinuum generation, we performed most of the simulation runs also with a higher group velocity dispersion parameter. It turns out that increasing GVD by an order of magnitude leads to a strong suppression of the continuum production. We speculate that it may be one of the reasons that, at least in some experiments, there is only little spectral broadening in the ultraviolet (UV) femtosecond pulses [27] because the GVD value of air is significantly higher in the UV region.

The findings from our numerical simulations should be accessible to experimental testing. However, extreme caution should be exercised when trying to compare experimental and simulational spectra. The spectra we present are taken from "one shot". They exhibit modulations typical for supercontinuum generation in gases [2,28]. While the characteristic "frequency" of the modulation is rather reproducible, the exact spectral shape is not. Thus, even small fluctuation in the parameters of the pulses will result in a suppression of fine features in the multiple-shot experimental spectra.

VII. CONCLUSIONS

We have performed a computer simulation study of the effects of the initial pulse polarization on its propagation and filamentation dynamics. In agreement with the experiment [17], we have found that the filamentation onset is reached earlier for a linearly polarized pulse than in a circularly polarized pulse of the same peak power. However, in some cases, the experiment indicates that the circularly polarized pulses create higher plasma densities in comparison with linearly polarized pulses. Our simulations suggest the opposite, but one has to keep in mind that the experimental measurements and our simulation pertain to rather different conditions, including much higher power and focusing in the experiment. In our simulations, we also see more self-focusing events with linearly polarized pulses than with circularly polarized ones.

We have observed a rich spatio-temporal polarization dynamics. Naturally, the limited range of the full parameter space explored in our simulations prevents us from drawing general conclusions, but we believe some tendencies are already discernible. First, the initially circular polarization seems to be stable in a sense that a small perturbation of the polarization state doesn't grow significantly. On the other hand, when a small polarization perturbation is applied to the linearly polarized pulse, it grows and the polarization degree of the central filament decreases significantly. The growth rate of the deviation is expected to increase for higher powers. An interesting case is the one of an initially elliptic polarization. We have observed that the center of the filament is almost purely circularly polarized after subsequent self-focusing collapses within the pulse. Apparently, we have here a rather different situation than in the self-focusing in nanosecond pulses, which tend to create linearly polarized filaments independently of initial polarization state [21,18]. The usual argument, that the the weaker circular component experiences stronger self-focusing which finally leads to balancing the power of the circularly polarized components and thus to linear polarization, can't be applied in the femtosecond pulses. The evolution of the polarization state along the propagation distance is extremely dynamic and hardly possible to describe in simple "static" terms. The multiple refocusing within a pulse and the defocusing effect of the generated plasma play a major role. The important feature of the whole process is that apart from the relatively small energy losses due to plasma generation and radiation, the energy in each circular component remains conserved. Thus, the main mechanism that results in changing polarization pattern within the pulse is the spatio-temporal energy redistribution within each circular component. As a consequence, the polarization state of the whole pulse is very complicated and, therefore, any projection onto global quantities like Stokes parameters has to be interpreted in relation to details of the measurement (aperture, near vs. far field, collecting angle, ...).

We have also looked at spectra "measured" after the last self-focusing collapse for different initial polarizations. In accordance with our observation about the plasma generation, we see much stronger supercontinuum generation in linearly polarized than in circularly polarized pulses.

Finally, we have seen that rate of change of the polarization state in the center of the filament is closely correlated with self-focusing and plasma generation. Thus, the polarization offers, in principle, an alternative way to investigate the dynamics of the spatial replenishment in femtosecond pulses.

In this work, we have concentrated on investigating "global" quantities to characterize the femtosecond pulse propagation that should be experimentally accessible, at least in principle. Naturally, the question is how much can be done practically. To measure the Stokes parameters evolution along the propagation distance, for example, a very good reproducibility of the initial pulse would be required. However, the "final output" polarization state and spectra, which should be easier to measure,

also carry a lot of signatures about the inner dynamics of the femtosecond pulse propagation.

VIII. ACKNOWLEDGMENTS

Work supported by AFOSR grant no. F4962-00-1-0312, AFOSR DURIP grant no. F4962-00-1-0190, and in part by Boeing. M.K. was partly supported by the GASR grant VEGA 2/7174/20.

[1] A. Braun *et al.*, Opt. Lett. **20**, 73 (1995).
[2] E. Nibbering *et al.*, Opt.Lett. **21**, 62 (1996).
[3] A. Brodeur *et al.*, Opt. Lett. **22**, 304 (1997).
[4] O. Kosareva *et al.*, Opt.Lett. **22**, 1332 (1997).
[5] H. Lange *et al.*, Opt. Lett. **23**, 120 (1998).
[6] L. Wöste *et al.*, AT-Fachverlag, Stuttgart, Laser und Optoelektronik **29**, 51 (1997).
[7] B. La Fontaine *et al.*, Phys. of Plasmas **6**, 1615 (1999).
[8] A. Talebpour, S. Petit, and S. Chin, Opt. Commun. **171**, 285 (1999).
[9] M. Mlejnek, E. Wright, and J. Moloney, Opt. Lett. **23**, 382 (1998).
[10] M. Mlejnek, E. Wright, and J. Moloney, Phys. Rev. E **58**, 4903 (1998).
[11] M. Mlejnek, E. Wright, and J. Moloney, IEEE J. Quant. Electron. **35**, 1771 (1999).
[12] M. Mlejnek, M. Kolesik, J. Moloney, and E. Wright, Phys. Rev. Lett. **83**, 2938 (1999).
[13] A. Chiron *et al.*, Eur. Phys. J. D **6**, 383 (1999).
[14] A. Couairon and L. Bergé, Phys. of Plasmas **7**, 193 (2000).
[15] L. Bergé and A. Couairon, Phys. of Plasmas **7**, 210 (2000).
[16] N. Aközbek, C. Bowden, A. Talebpour, and L. Chin, Phys. Rev. E **61**, 4540 (2000).
[17] S. Petit, A. Talebpour, A. Proulx, and S. Chin, Opt. Commun. **175**, 323 (2000).
[18] J. Marburger, in *Prog. Quant. Elect.* (Pergamon Press, Oxford, 1977), Vol. 4, p. 35.
[19] L. Keldysh, Sov. Phys. JETP **20**, 1307 (1965).
[20] B. Daino, G. Gregori, and S. Wabnitz, Opt. Lett. **11**, 42 (1986).
[21] Y. Shen, in *Prog. Quant. Elect.* (Pergamon Press, Oxford, 1977), Vol. 4, p. 1.
[22] M. Kolesik, M. Mlejnek, J. Moloney, and E. Wright, in *Optical pulse and beam propagation II*, Vol. 3927 of *Proceedings of SPIE*, edited by Y. Band (SPIE, Bellingham, 2000), p. 81.
[23] H. Schillinger and R. Sauerbrey, Appl. Phys.B **68**, 753 (1999).
[24] C. Chien *et al.*, Opt. Lett. **25**, 578 (2000).
[25] S. Tzortzakis *et al.*, Phys. Rev. E **60**, R3505 (1999).
[26] T. Brabec and F. Krausz, Phys. Rev. Lett. **78**, 3282 (1997).
[27] J. Schwartz *et al.*, Opt. Commun. **180**, 383 (2000).
[28] P. Corkum and C. Rolland, in *The supercontinuum laser source*, edited by R. Alfano (Springer, New York, 1989), p. 318.

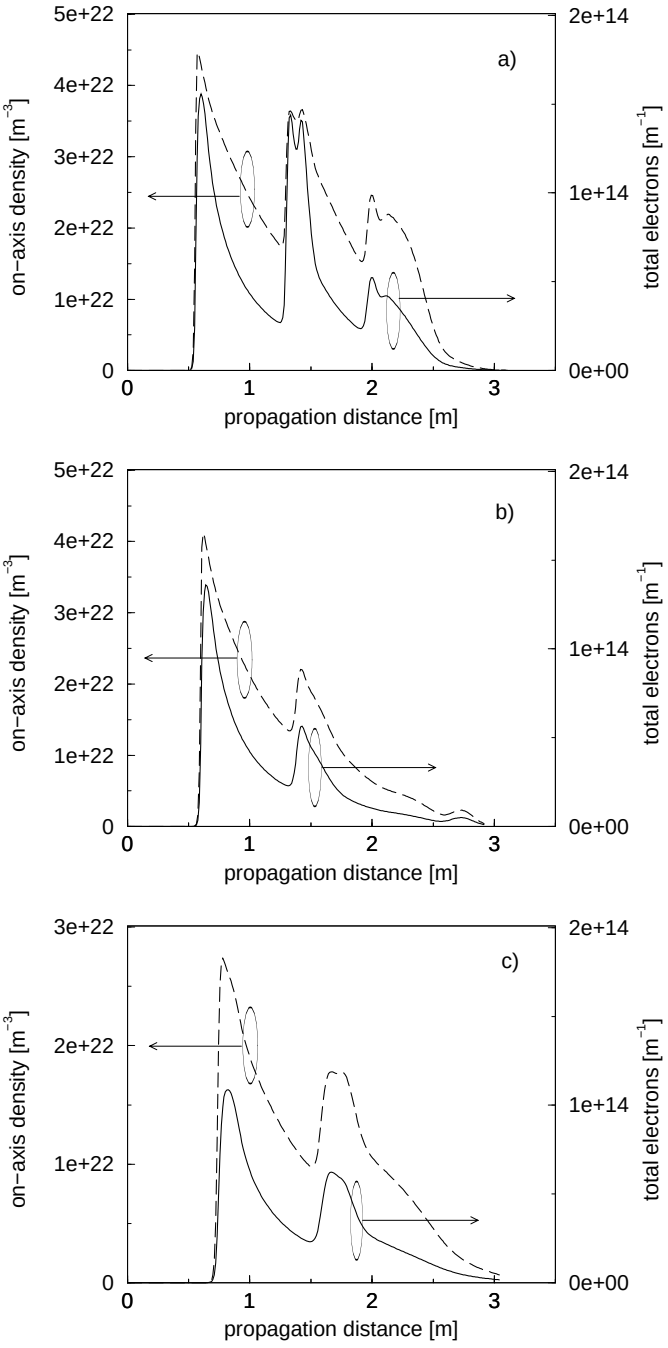

FIG. 1. Plasma generation for almost linear (a), elliptic (b) and a close-to-circular (c) initial pulse polarization. The total peak power is kept the same in all cases. Since the critical power for self-focusing is higher for circular polarization, the circularly polarized pulse experiences weaker self-focusing which in turn results in less overall plasma generation.

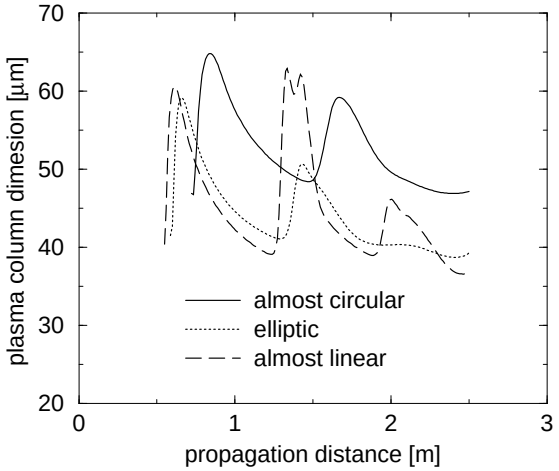

FIG. 2. Characteristic transverse dimension of the generated plasma column for three different initial polarizations.

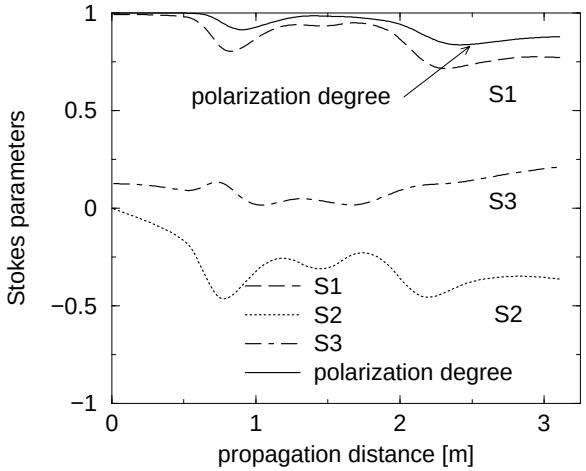

FIG. 3. Stokes polarization parameters of the on-axis part of the pulse as functions of the propagation distance for an almost linear initial polarization. The initial deviation from the perfect linear polarization increases, and the polarization degree decreases.

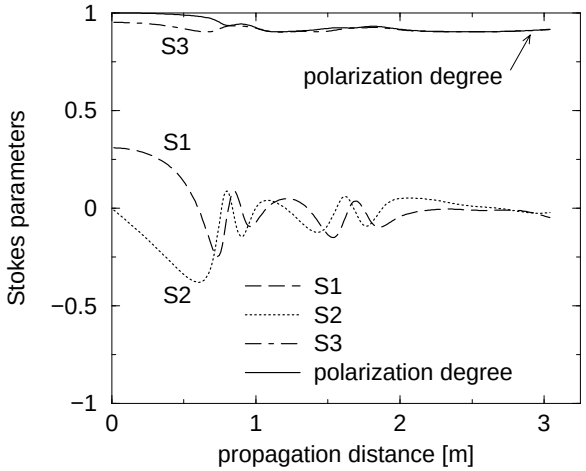

FIG. 4. An initially almost circularly polarized pulse (approximately) preserves its polarization state. There is only a slight decrease of the polarization degree.

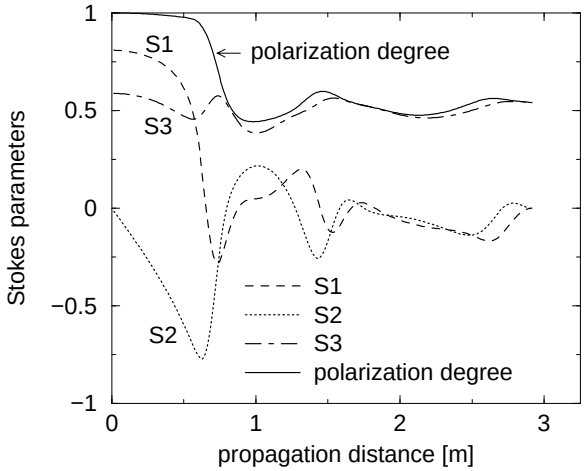

FIG. 5. Stokes polarization parameters as functions of the propagation distance for an elliptic initial polarization of the pulse. The central part of the filament evolves into a predominantly circular polarization state after the second self-focusing collapse event. Note that the rate of change of the polarization state correlates with the loci of maximal plasma production (see Fig. 6).

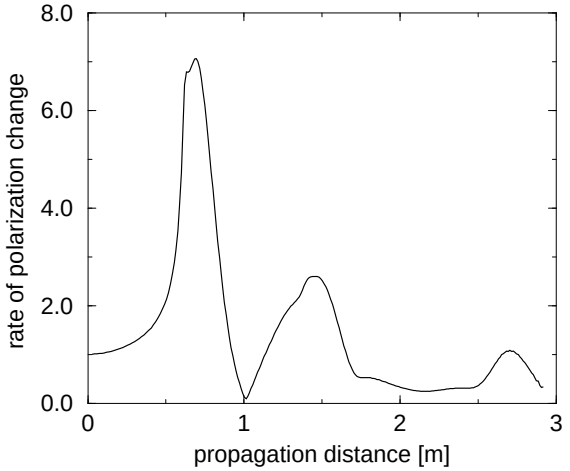

FIG. 6. Root-mean-square of the rate of change of the Stokes polarization vector, ds/dz (in units of m^{-1}) as a function of the propagation distance for elliptic initial polarization. The rate maxima are correlated with the locations of strongest plasma generation and focusing.

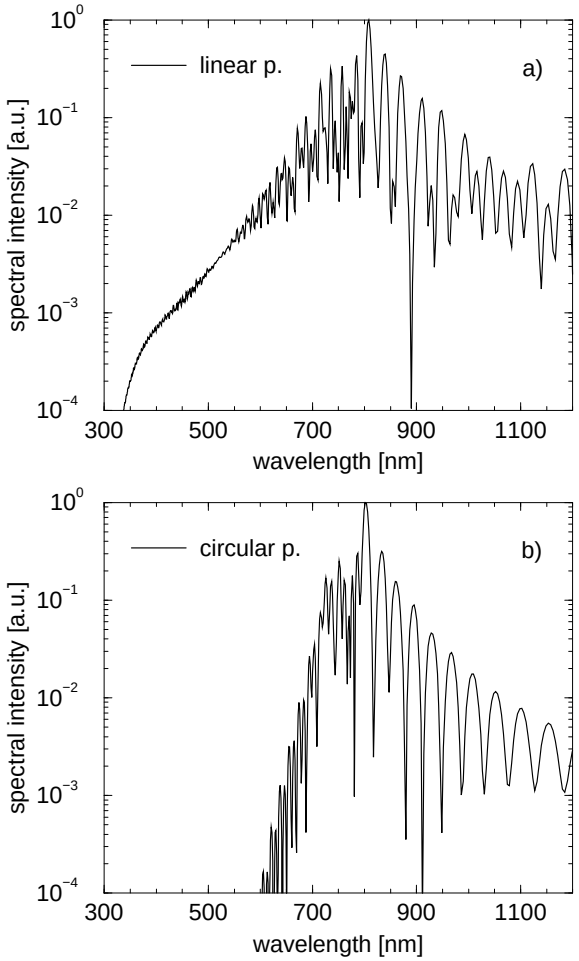

FIG. 7. Spectral broadening of two femtosecond pulses with different initial polarizations. The linearly polarized pulse produces significantly more supercontinuum light than an equally intense circularly polarized pulse.

TABLE I. Model parameters and numerical values used in our simulations.

Quant.	Value&Unit	Note
k	$k = 2\pi/\lambda_0$	reference wavevector
λ_0	775×10^{-9} m	wavelength
k''	2.1×10^{-29} s^2/m	group velocity dispersion
n_2	5.6×10^{-19} cm^2/W	nonlinear index
f	0.5	
Γ	26 THz	$R(t) \sim \theta(t)\times$
Λ	16 THz	$e^{-\Gamma t/2}\sin(\Lambda t)$
K	7	MPI order
E_g	≈ 11 eV	ionization energy
β_K	6.5×10^{-104} m^{11}W^{-6}	MPI rate
τ	3.5×10^{-13} s	electron collision time
σ	5×10^{-24} m^2	cross-section for inverse bremsstrahlung
a	5×10^{-13} m^3/s	recombination rate